

Gate-tunable high-responsivity photodiode based on 2D ambipolar semiconductor

Wentao Yu(于文韬), Long Zhao(赵龙), Yanfei Gao(高延飞), Shiping Gao(高石平), Yuekun Yang(杨悦昆), Chen Pan(潘晨), Shi-Jun Liang(梁世军), and Bin Cheng(程斌)

Citation: Chin. Phys. B, 2025, 34 (**1**): 018502. DOI: 10.1088/1674-1056/ad9c44

What follows is a list of articles you may be interested in

Recent progress on two-dimensional ferroelectrics: Material systems and device applications

Zhiwei Fan(范芷薇), Jingyuan Qu(渠靖媛), Tao Wang(王涛), Yan Wen(温艳), Ziwen An(安子文), Qitao Jiang(姜琦涛), Wuhong Xue(薛武红), Peng Zhou(周鹏), and Xiaohong Xu(许小红)

Chin. Phys. B, 2023, 32 (**12**): 128508. DOI: 10.1088/1674-1056/ad08a4

A fast-response self-powered UV-Vis-NIR broadband photodetector based on a $AgIn_5Se_8$/t-Se heterojunction

Kang Li(李康), Lei Xu(许磊), Qidong Lu(陆启东), and Peng Hu(胡鹏)

Chin. Phys. B, 2023, 32 (**11**): 118503. DOI: 10.1088/1674-1056/acec44

Novel layout design of 4H-SiC merged PiN Schottky diodes leading to improved surge robustness

Jia-Hao Chen(陈嘉豪), Ying Wang(王颖), Xin-Xing Fei(费新星), Meng-Tian Bao(包梦恬), and Fei Cao(曹菲)

Chin. Phys. B, 2023, 32 (**9**): 098505. DOI: 10.1088/1674-1056/acad6b

A SiC asymmetric cell trench MOSFET with a split gate and integrated p^+-poly Si/SiC heterojunction freewheeling diode

Kaizhe Jiang(蒋铠哲), Xiaodong Zhang(张孝冬), Chuan Tian(田川), Shengrong Zhang(张升荣),Liqiang Zheng(郑理强), Rongzhao He(赫荣钊), and Chong Shen(沈重)

Chin. Phys. B, 2023, 32 (**5**): 058504. DOI: 10.1088/1674-1056/acbd2d

Low switching loss and increased short-circuit capability split-gate SiC trench MOSFET with p-type pillar

Pei Shen(沈培), Ying Wang(王颖), Xing-Ji Li(李兴冀), Jian-Qun Yang(杨剑群), and Fei Cao(曹菲)

Chin. Phys. B, 2023, 32 (**5**): 058501. DOI: 10.1088/1674-1056/ac98a1

RAPID COMMUNICATION

Gate-tunable high-responsivity photodiode based on 2D ambipolar semiconductor

Wentao Yu(于文韬)[1], Long Zhao(赵龙)[1], Yanfei Gao(高延飞)[1], Shiping Gao(高石平)[1], Yuekun Yang(杨悦昆)[2], Chen Pan(潘晨)[1,†], Shi-Jun Liang(梁世军)[2,‡], and Bin Cheng(程斌)[1,§]

[1] *Institute of Interdisciplinary Physical Sciences, School of Physics, Nanjing University of Science and Technology, Nanjing* 210094, *China*

[2] *Institute of Brain-Inspired Intelligence, National Laboratory of Solid State Microstructures, School of Physics, Collaborative Innovation Center of Advanced Microstructures, Jiangsu Physical Science Research Center, Nanjing University, Nanjing* 210093, *China*

(Received 12 November 2024; revised manuscript received 4 December 2024; accepted manuscript online 10 December 2024)

Electrically tunable homojunctions based on ambipolar two-dimensional materials have attracted widespread attention in the field of intelligent vision. These devices exhibit inherent switchable positive and negative photovoltaic properties that effectively mimic the behavior of human retinal cells. However, the photovoltaic responsivity of most electrically tunable homojunctions remains significantly low due to the weak light absorption, making it challenging to meet the application requirements for high-sensitivity target detection in the field of intelligent vision. Here, we propose a gate-tunable photodiode based on two-dimensional ambipolar WSe_2 with an asymmetric gate electrode, achieving high photovoltaic responsivity. By adjusting the gate voltage and keeping bias voltage zero, we can dynamically realize reconfigurable n^-–p and n^-–n homojunction states, as well as gate-tunable photovoltaic response characteristics that range from positive to negative. The maximum photovoltaic responsivity of the electrically tunable WSe_2 homojunction is approximately 0.4 A/W, which is significantly larger than the previously reported value $\sim$ 0.1 A/W in homojunction devices. In addition, the responsivity can be further enhanced to approximately 1.0 A/W when the n^-–p photodiode operates in reverse bias mode, enabling high-sensitivity detection of targets. Our work paves the way for developing gate-tunable photodiodes with high photovoltaic responsivity and advancing high-performance intelligent vision technology.

Keywords: reconfigurable homojunction, in sensor computing, ambipolar material

PACS: 85.30.−z, 85.60.Gz

DOI: 10.1088/1674-1056/ad9c44 **CSTR:** 32038.14.CPB.ad9c44

1. Introduction

Recently, the rapid development of two-dimensional (2D) material photodetectors has significantly advanced the future of intelligent vision technology.[1–12] These advancements stem from the fact that 2D materials not only exhibit excellent photoelectric response characteristics, but also these properties can also be effectively and dynamically controlled by electrical fields.[13–19] The superior performance of 2D materials is attributed to their intrinsic properties, including strong light–matter interactions and atomic thickness.[20–23] In particular, a class of 2D materials exhibit ambipolar properties, allowing for effective control of their majority carrier types and concentrations through the bias voltage[24] or the gate voltage.[18,25–27] Furthermore, for the same ambipolar material, by utilizing the multi-gate device structure, the electrostatic doping states in different regions of the material can be differentially regulated.[28–31] This allows for dynamically tunable homojunction properties, enabling the device to exhibit switchable positive and negative photovoltaic characteristics and work as gate-tunable photodiodes,[25,26,32–34] which are essential for achieving intelligent vision applications.[15,35–37] However, photovoltaic responsivity demonstrated in those previous works on electrically tunable homojunction is still significantly low due to weak light absorption in the homojunction area.[25,26] This discrepancy limits the ability to achieve high-sensitivity target detection and hampers practical application in the field of intelligent vision.

In this work, we propose a gate-tunable photodiode based on 2D ambipolar WSe_2, exhibiting high photovoltaic responsivity under zero bias mode. We fabricated a field-effect transistor in which the gate electrode overlaps only the source region. This design allows the gate to dynamically switch the doping state of the source region while maintaining the doping state of the drain region in the material's intrinsic state. By applying different gate voltages, we can modulate the device state between n^-–p and n^-–n homojunction configurations. This capacity enables the demonstration of gate-tunable photovoltaic response characteristics that range from positive to negative. We demonstrate that the device has an ultrahigh pho-

†Corresponding author. E-mail: chenpan@njust.edu.cn

‡Corresponding author. E-mail: sjliang@nju.edu.cn

§Corresponding author. E-mail: bincheng@njust.edu.cn

© 2025 Chinese Physical Society and IOP Publishing Ltd. All rights, including for text and data mining, AI training, and similar technologies, are reserved.

tovoltaic responsivity of approximately 0.4 A/W under 532-nm light illumination and zero bias voltage, near 4-fold enhancement compared with the reported value ∼ 0.1 A/W based on the electrically tunable WSe_2 homojunction.[34] By changing the device's operating state to the n^-–p photodiode reverse bias mode, its responsivity can be enhanced to approximately 1.0 A/W, offering significant potential for high-sensitivity target detection. Our work explores a novel approach to achieving both dynamically tunable photovoltaic characteristics and high photovoltaic responsivity, which is expected to advance high-performance intelligent vision applications.

2. Method

Device fabrication began with the mechanical exfoliation of WSe_2 and h-BN on the silicon substrate. The bottom gate electrode (Cr/Au, 5 nm/40 nm) was fabricated on the SiO_2 (300 nm)/Si substrates via electron beam lithography and electron beam evaporation. A hexagonal boron nitride (h-BN) flake (∼ 20 nm) was then transferred onto the gate electrode using the polymer vinyl alcohol (PVA) transfer method as the dielectric layer. Subsequently, a WSe_2 flake (∼ 15 nm) was stacked on the h-BN, and source and drain electrodes (Cr/Au, 5 nm/40 nm) were fabricated on top of the WSe_2 flake. It is important to note that the as-fabricated gate electrode should only overlap with half of the WSe_2 channel between the source and drain electrodes. These materials were confirmed by Raman spectroscopy using a microscopic Raman spectrometer (Witec alpha 300) with a 532-nm laser as the excited light.

We focused 532 nm light through the home-made microscope system equipped with a long-work-distance objective lens to the sample. The laser spot size was ∼ 1.5 μm in diameter. The voltage and current measurements were performed using a source measurement unit (Keithley, 2636B) and an Agilent B1500A parameter analyzer. All the measurements were performed in vacuum environment (∼ 10^{-6} mbar) at room temperature.

3. Result and discussion

The structure of the proposed gate-tunable photodiode (GTP) based on 2D WSe_2 with an asymmetric gate electrode is illustrated in Fig. 1(a). In our device, a WSe_2 flake (∼ 15 nm) is used as the photosensitive material, while a hexagonal boron nitride (h-BN) flake (∼ 20 nm) is chosen as the dielectric layer due to its atomically flat surface and charge trap-free interface. The asymmetric gate electrode (Cr/Au, 5 nm/40 nm) overlaps only with the source region of the WSe_2 channel between the top source and drain electrodes (Cr/Au, 5 nm/40 nm), as shown in the optical image of Fig. 1(b). This design ensures that the gate voltage (V_g) adjusts the doping state of the source region while leaving the doping state of the drain region unchanged, thus maintaining its intrinsic state. Consequently, the device can exhibit gate-tunable homojunction characteristics.

These materials were confirmed by Raman spectroscopy, as illustrated in Fig. 1(c). In the WSe_2/h-BN region, the Raman peak near 1365 cm^{-1} corresponds to the E_{2g} mode of h-BN, which is also observed in the h-BN area.[38] Additionally, a prominent peak at 250 cm^{-1} (A_{1g} mode of WSe_2) with a shoulder near 257 cm^{-1} (E_{2g} mode of WSe_2) further confirms the materials used in our device.[39] To investigate the initial doping state of WSe_2, we fabricated a global back-gate WSe_2 field-effect transistor and obtained the expected ambipolar field-effect transfer curve, as shown in Fig. S1. The initial doping state of WSe_2 is confirmed to be weakly n-doped (n^-) with the applied gate voltage set at 0 V.

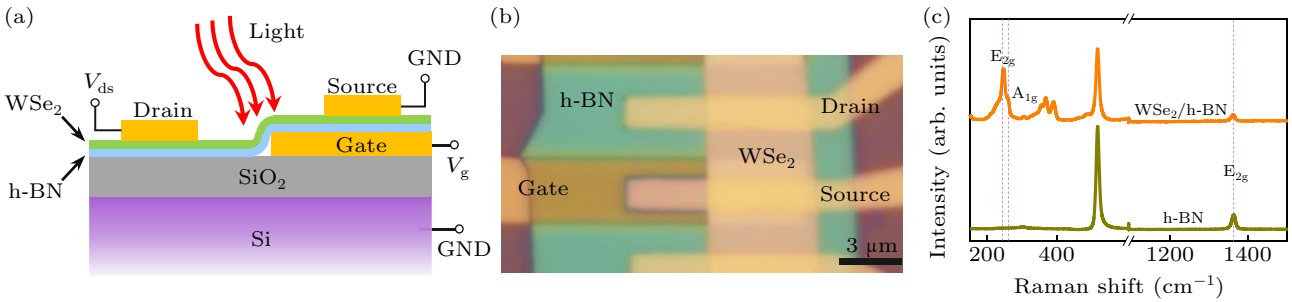


Fig. 1. The structure of the gate tunable photodiode. (a) Schematic of WSe_2 photodetector with asymmetric gate. The drain–source bias V_{ds} and gate voltage V_g can be applied to modulate the working state with the source grounded (GND). The Si substrate is also grounded. (b) The optical image of a representative device, the scale bar is 3 μm. (c) Raman spectra at different positions of the WSe_2/h-BN and h-BN.

The proposed GTP can be modulated as an n^-–p homojunction or n^-–n homojunction with a negative or positive V_g. When a negative V_g is applied to the gate electrode, it induces a p-doped state in the channel material above the gate electrode near the source terminal. In contrast, the channel material near the drain electrode, which does not overlap with the gate electrode, remains in an intrinsic n^--doped state. As a result, an n^-–p homojunction is formed, and the corresponding band diagram is depicted in the bottom panel of Fig. 2(a). The I_{ds}–V_{ds} curve for the n^-–p homojunction is shown as the red curve in Fig. 2(c), achieving a high rectification ratio over 10^3. When a positive V_g is applied to the gate electrode, the

channel material above it can be regulated to become n-doped, thereby forming an n$^-$–n homojunction. The corresponding band diagram and the measured I_{ds}–V_{ds} curve for this configuration are shown in the bottom panel of Fig. 2(b) and as the blue curve in Fig. 2(c), respectively. Since the built-in field strength of the n$^-$–n junction is weaker than that of the n$^-$–p junction, the rectification ratio of the I_{ds}–V_{ds} curve is only 10^2, which is lower than that of the n$^-$–p junction. Consequently, the measured I_{ds}–V_{ds} curves confirm the characteristics of the proposed gated tunable homojunction device.

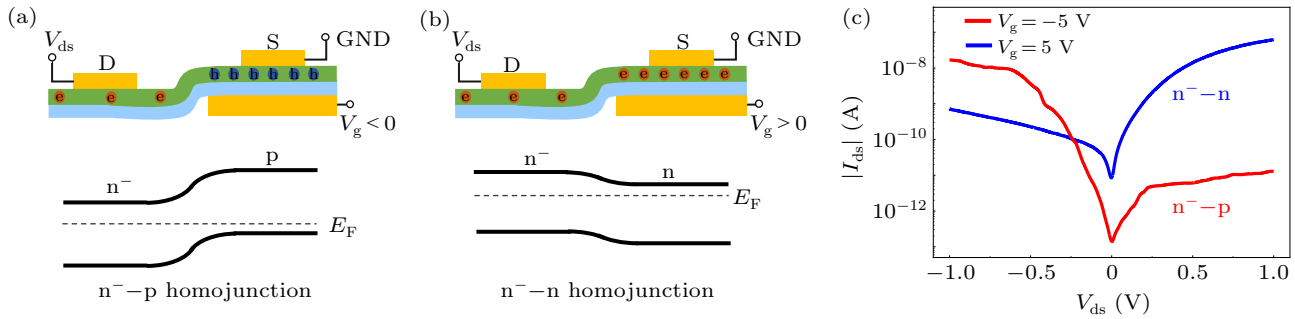


Fig. 2. The gate-tunable homojunction behaviors. [(a) and (b)] Operation diagrams of n$^-$–p and n$^-$–n homojunctions with negative and positive V_g applied (top panel), and the corresponding band diagrams (bottom panel). D, S and E_F mean drain, source and Fermi level, respectively. (c) Semilog plot of output curves ($|I_{ds}|$–V_{ds}) for n$^-$–p junction ($V_g = -5$ V) and n$^-$–n junctions ($V_g = 5$ V).

The demonstrated tunable homojunction behaviors provide an ideal platform for showcasing a gate-tunable photodiode with high photovoltaic responsivity. A light source (532 nm) was focused on the junction region of the WSe_2 device, and the light spot had a diameter of approximately 1.5 μm. The photo-generated electrons and holes in the WSe_2 homojunction were expected to be separated by the built-in electric field, resulting in a short-circuit current (I_{sc}) and open-circuit voltage (V_{oc}). Considering that the light spot was smaller than the size of the whole WSe_2 channel and focused on the junction area, the electrical outputs (I_{sc} and V_{oc}) were thought to be attributed to the contributions of the WSe_2 homojunction, rather than the Schottky junctions near the drain/source electrodes.

The proposed GTP exhibited inherent photovoltaic properties with high photoelectric conversion efficiency. In Fig. 3(a), we measured the basic optoelectronic characteristics of the device, presenting the output curves ($|I_{ds}|$–V_{ds}) in the dark and at various light power levels (P_{in}) on a semi-logarithmic scale with V_g set to −5 V (n$^-$–p junction). The corresponding output curves in linear scale are shown in Fig. S2. As P_{in} increases, both I_{sc} and V_{oc} gradually deviate from zero, indicating a significant photovoltaic effect. The I_{sc} and V_{oc} as functions of P_{in} were extracted and presented in Fig. 3(b), both showing monotonical increase with P_{in}. The I_{sc}–P_{in} data was fitted using the power relationship $I_{sc} \sim P_{in}^{\alpha}$, yielding $\alpha = 0.98$. The nearly linear dependence between I_{sc} and P_{in} indicates that the photovoltaic effect dominates the photocurrent generation.[40,41] Additionally, V_{oc} exhibits a logarithmic dependence on P_{in} when P_{in} is lower than 10^{-7} W and demonstrates saturation behavior with higher P_{in} level. The generated electrical power ($P_{el} = |I_{ds} \times V_{ds}|$) increases with light power and reaches 144 nW at $P_{in} = 1.30$ μW with $V_{ds} = -0.36$ V, as shown in Fig. S3. Hence, the maximum power conversion efficiency (PCE $= P_{el,max}/P_{in}$) reaches $\sim 11\%$ at $P_{in} = 1.30$ μW, as shown in Fig. S4. The maximum is larger than the reported values,[25,26,34] indicating the high-efficiency conversion from light power to electrical output signal and possible high responsivity.

Then, we characterized the GTP device as having a periodic, stable, and tunable photoresponse. In Fig. 3(c), we observed a periodically switched photocurrent without severe degradation under zero bias voltage and $V_g = -5$ V, which ensured good stability and reproducibility of the photovoltaic response of our device. Under illumination power of 1.30 μW, the I_{sc} reached about 510 nA, accompanied by a low dark current of 10^{-12}–10^{-13} A. Furthermore, while maintaining a constant zero bias voltage and varying the gate voltage (V_g) from 5 V to −5 V, the photocurrent varied from −12.5 nA to +51.5 nA with the light power of 130 nW, as shown in Fig. 3(d), where the positive direction of the photocurrent was defined from the drain to the source. The tunable photoresponses observed with different V_g were attributed to the varying homojunction conditions. When $V_g > 0$, our device worked as an n$^-$–n junction, and the direction of the built-in electric field was from the source to the drain, resulting in a negative photocurrent. As V_g decreased to −5 V, the junction changed from n$^-$–n to n$^-$–p mode, leading to a change in the built-in electric field direction from negative to positive, which resulted in a tunable photocurrent ranging from negative to positive values, as shown in Fig. S5.

To clearly illustrate the advantages of the proposed GTP device, we extracted its photoresponse parameters based on the application requirements for photoelectric sensing. For practical applications, high responsivity and a high light on/off ratio of the photodiode are critical for the sensitive detection

of dim targets with low dark noise. Responsivity is defined as I_{ph}/P_{in}, and the light on/off ratio is I_{ph}/I_{dark}, where I_{dark} represents the dark current (the current measured in the absence of light) and I_{ph} is the photocurrent (the difference between the measured current and the dark current). Under zero bias voltage and $V_g = -5$ V, the responsivity reaches nearly constant at approximately 0.4 A/W across the used light power, as shown in Fig. 3(e). This photovoltaic responsivity is about 4 times higher than the reported value ~ 0.1 A/W based on the electrically tunable WSe_2 homojunction.[34] The high responsivity is attributed to the improvement of light absorption near the edge region of the asymmetric gate electrode due to local light field enhancement.[42,43] Besides, since the edge region of the gate electrode overlaps with the homojunction area, photo-induced carriers can be efficiently separated by the built-in electric field, leading to a large photocurrent and resulting in high responsivity. Accompanied by the low dark current, the high light on/off ratio can exceed 10^6 with $P_{in} = 1.30$ μW, as shown in Fig. 3(e). In addition, when V_{ds} is set to 1 V to form a reversed-biased n^-–p junction, the responsivity can be further enhanced to nearly 1 A/W at low light power, as shown in Fig. 3(f). Under illumination and a reverse bias of $V_{ds} = 1$ V, the photo-induced carriers are rapidly swept in opposite directions by the junction electric field and the additional reverse-bias electric field. As a result, both the reverse current and the responsivity increase due to the internal gain provided by the reverse-bias electric field, compared to the zero-bias mode. This enhanced responsivity could significantly improve the photodiode's capacity for dim target detection. The tunable high-performance photovoltaic photodetector based on the WSe_2 homojunction shows the enormous potential in the field of visual sensing.

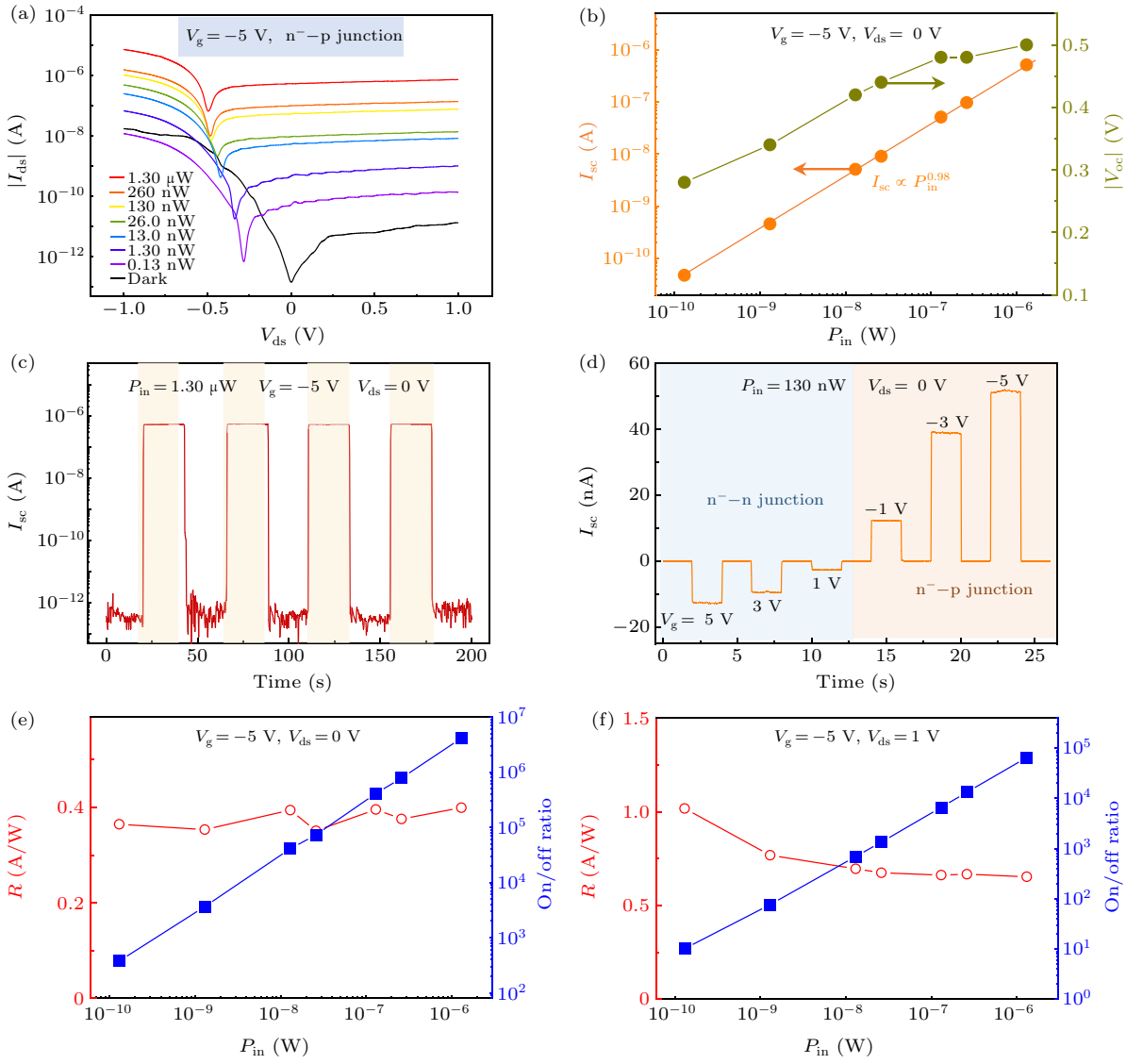


Fig. 3. The high-performance and tunable photoresponse. (a) Semilog plot of output curves ($|I_{ds}|$–V_{ds}) for n^-–p junction with different light power (P_{in}) with wavelength at 532 nm. (b) Extracted short-circuit current (I_{sc}) and open-circuit voltage (V_{oc}) under different P_{in}. (c) Time-resolved I_{sc} under periodic light illumination for $P_{in} = 1.30$ μW. (d) Time-resolved gate-tunable I_{sc} at different V_g for $P_{in} = 130$ nW. [(e) and (f)] Responsivity (R) and light on/off ratio under different P_{in} at zero bias ($V_{ds} = 0$ V) and negative bias ($V_{ds} = 1$ V) for n^-–p junction, respectively.

4. Conclusion and perspectives

We presented a gate-tunable photodiode with high photovoltaic responsivity under zero bias mode by utilizing two-dimensional ambipolar WSe_2 combined with an asymmetric gate structure. In this device, the gate voltage dynamically alters the doping state of the source channel, while the drain's doping state remains in its intrinsic state. This allows us to achieve dynamically reconfigurable n^-–p and n^-–n homojunction states. Leveraging this tunable homojunction property, we demonstrated a tunable photovoltaic response that varies from positive to negative. We have successfully demonstrated that the device exhibits an ultrahigh photovoltaic responsivity of up to ~ 0.4 A/W under zero bias mode. Furthermore, the responsivity can be enhanced to approximately 1.0 A/W when the n^-–p photodiode operates in reverse bias mode. These results indicate a promising approach for achieving high-sensitivity target detection and are expected to promote the development of high-performance intelligent vision technology.

Acknowledgments

Project supported by the National Natural Science Foundation of China (Grant Nos. 62375131, 62204119, 62122036, and 62304104), the Natural Science Foundation of Jiangsu Province (Grant No. BK20220947), and the Funding of NJUST (Grant No. TSXK2022D008).

References

[1] Wang S, Wang C Y, Wang P F, Wang C, Li Z A, Pan C, Dai Y T, Gao A Y, Liu C, Liu J, Yang H F, Liu X W, Cheng B, Cheng K J, Wang Z L, Watanabe K, Taniguchi T, Liang S J and Miao F 2021 *Natl. Sci. Rev.* **8** nwaa172

[2] Peng Z R, Tong L, Shi W H, Xu L L, Huang X Y, Li Z, Yu X X, Meng X H, He X, Lv S J, Yang G C, Hao H, Jiang T, Miao X S and Ye L 2024 *Nat. Commun.* **15** 8650

[3] Zhang Z, Wang S, Liu C, Xie R, Hu W and Zhou P 2021 *Nat. Nanotechnol.* **17** 27

[4] Shang H, Hu Y, Gao F, Dai M, Zhang S, Wang S, Ouyang D, Li X, Song X, Gao B, Zhai T and Hu P 2022 *ACS Nano* **16** 21293

[5] Pan X, Shi J W, Wang P F, Wang S, Pan C, Yu W T, Cheng B, Liang S J and Miao F 2023 *Sci. Adv.* **9** eadi4083

[6] Yang Y, Pan C, Li Y, Yangdong X, Wang P, Li Z A, Wang S, Yu W, Liu G, Cheng B, Di Z, Liang S J and Miao F 2024 *Nat. Electron.* **7** 225

[7] Dang Z Y, Guo F, Wang Z Q, Jie W J, Jin K, Chai Y and Hao J H 2024 *ACS Nano* **18** 27727

[8] Cai Y C, Wang F, Wang X M, Li S H, Wang Y R, Yang J, Yan T, Zhan X Y, Wang F M, Cheng R Q, He J and Wang Z X 2023 *Adv. Funct. Mater.* **33** 2212917

[9] Zeng S, Liu C, Huang X, Tang Z, Liu L and Zhou P 2022 *Nat. Commun.* **13** 56

[10] Feng G, Zhang X, Tian B and Duan C 2023 *InfoMat* **5** e12473

[11] Yang Y, Zhao J, Liu Y, Hua X, Wang T, Zheng J, Hao Z, Xiong B, Sun C, Han Y, Wang J, Li H, Wang L and Luo Y 2024 *Chin. Phys. B* **33** 030702

[12] Wang H, Song X, Li Z, Li D, Xu X, Chen Y, Liu P, Zhou X and Zhai T 2024 *J. Semicond.* **45** 051701

[13] Wang C Y, Liang S J, Wang S, *et al.* 2020 *Sci. Adv.* **6** eaba6173

[14] Liao F, Zhou Z, Kim B J, Chen J, Wang J, Wan T, Zhou Y, Hoang A T, Wang C, Kang J, Ahn J H and Chai Y 2022 *Nat. Electron.* **5** 84

[15] Zhou Y, Fu J W, Chen Z R, Zhuge F W, Wang Y S, Yan J M, Ma S J, Xu L, Yuan H M, Chan M S, Miao X S, He Y H and Chai Y 2023 *Nat. Electron.* **6** 870

[16] Jin H, Park C, Byun H H, Park S H and Choi S Y 2023 *ACS Photonics* **10** 3027

[17] Masanta S, Nayak C, Agarwal P, Das K and Singha A 2023 *ACS Appl. Mater. Interfaces* **15** 14523

[18] Liu F, Lin X, Yan Y T, Gan X T, Cheng Y C and Luo X G 2023 *Nano Lett.* **23** 11645

[19] Yang Y K, Wang X D, Wang C, Song Y X, Zhang M, Xue Z Y, Wang S M, Zhu Z Y S, Liu G Y, Li P L, Dong L X, Mei Y F, Chu W D, Hu J L, Wang and Di Z F 2020 *Nano Lett.* **20** 3872

[20] Mak K F and Shan J 2016 *Nat. Photon.* **10** 216

[21] Mak K F, Lee C, Hone J, Shan J and Heinz T F 2010 *Phys. Rev. Lett* **105** 136805

[22] Xie C, Mak C, Tao X M and Yan F 2017 *Adv. Funct. Mater.* **27** 1603886

[23] Jariwala D, Davoyan A R, Wong J and Atwater H A 2017 *ACS Photonics* **4** 2962

[24] Wei X, Yan F G, Lv Q S, Shen C and Wang K Y 2017 *Nanoscale* **9** 8388

[25] Baugher B W H, Churchill H O H, Yang Y F and Jarillo-Herrero P 2014 *Nat. Nanotechnol.* **9** 262

[26] Pospischil A, Furchi M M and Mueller T 2014 *Nat. Nanotechnol.* **9** 257

[27] Zhao Y, Sun H, Sheng Z, Zhang W, Zhou P and Zhang Z 2023 *Chin. Phys. B* **32** 128505

[28] Resta G V, Balaji Y, Lin D, Radu I P, Catthoor F, Gaillardon P E and De Micheli G 2018 *ACS Nano* **12** 7039

[29] Wu P, Reis D, Hu X B S and Appenzeller J 2021 *Nat. Electron.* **4** 45

[30] Pan C, Wang C Y, Liang S J, Wang Y, Cao T J, Wang P F, Wang C, Wang S, Cheng B, Gao A Y, Liu E F, Watanabe K, Taniguchi T and Miao F 2020 *Nat. Electron.* **3** 383

[31] Wu G J, Tian B B, Liu L, *et al.* 2020 *Nat. Electron.* **3** 43

[32] Ross J S, Klement P, Jones A M, Ghimire N J, Yan J Q, Mandrus D G, Taniguchi T, Watanabe K, Kitamura K, Yao W, Cobden D H and Xu X D 2014 *Nat. Nanotechnol.* **9** 268

[33] Liu T, Xiang D, Zheng Y, Wang Y A, Wang X Y, Wang L, He J, Liu L and Chen W 2018 *Adv. Mater.* **30** 1804470

[34] Li D, Chen M Y, Sun Z Z, Yu P, Liu Z, Ajayan P M and Zhang Z X 2017 *Nat. Nanotechnol.* **12** 901

[35] Wu G J, Zhang X M, Feng G D, Wang J L, Zhou K J, Zeng J H, Dong D N, Zhu F D, Yang C K, Zhao X M, Gong D N, Zhang M R, Tian B B, Duan C A, Liu Q, Wang J L, Chu J H and Liu M 2023 *Nat. Mater.* **22** 1499

[36] Mennel L, Symonowicz J, Wachter S, Polyushkin D K, Molina-Mendoza A J and Mueller T 2020 *Nature* **579** 62

[37] Han Z, Zhang Y C, Mi Q, You J, Zhang N N, Zhong Z Y, Jiang Z M, Guo H, Hu H Y, Wang L M and Zhu Z M 2024 *ACS Nano* **18** 29968

[38] Gorbachev R V, Riaz I, Nair R R, Jalil R, Britnell L, Belle B D, Hill E W, Novoselov K S, Watanabe K, Taniguchi T, Geim A K and Blake P 2011 *Small* **7** 465

[39] del Corro E, Terrones H, Elias A, Fantini C, Feng S M, Nguyen M A, Mallouk T E, Terrones M and Pimenta M A 2014 *ACS Nano* **8** 9629

[40] Xu J P, Luo X G, Hu S Q, Zhang X, Mei D, Liu F, Han N N, Liu D, Gan X T, Cheng Y C and Huang W 2021 *Adv. Mater.* **33** 2008080

[41] Buscema M, Island J O, Groenendijk D J, Blanter S I, Steele G A, van der Zant H S J and Castellanos-Gomez A 2015 *Chem. Soc. Rev.* **44** 3691

[42] Liu C, Ma C J, Gong D W, Ma C J, Chen D X, Wu C C, Zhao M Z, Zhang Z B, Yun J M, Xiao F J, Wang E E, Liu K H and Hong H 2023 *J. Phys. Chem. Lett.* **14** 5573

[43] Zhou S R, Fan H D, Wen S F, Zhang R, Yin Y, Lan C Y, Li C and Liu Y 2024 *Adv. Opt. Mater.* **12** 2301982